Dalton Transactions

RSC Publishing

PAPER

View Article Online
View Journal | View Issue

Cite this: *Dalton Trans.*, 2013, **42**, 3533

# Catalytic amine-borane dehydrogenation by a PCP-pincer palladium complex: a combined experimental and DFT analysis of the reaction mechanism†‡

Andrea Rossin,*[a] Giovanni Bottari,[b] Ana M. Lozano-Vila,[b] Margarita Paneque,*[b] Maurizio Peruzzini,*[a] Andrea Rossi[a] and Fabrizio Zanobini[a]

Received 27th September 2012,
Accepted 4th December 2012

DOI: 10.1039/c2dt32273k

**www.rsc.org/dalton**

Catalytic dehydrogenation of ammonia-borane ($NH_3{\cdot}BH_3$, AB) and dimethylamine borane ($NHMe_2{\cdot}BH_3$, DMAB) by the $Pd^{II}$ complex [($^{tBu}$PCP)Pd($H_2O$)]$PF_6$ [$^{tBu}$PCP = 2,6-$C_6H_3(CH_2P^tBu_2)_2$] leads to oligomerization and formation of spent fuels of general formula *cyclo*-$[BH_2–NR_2]_n$ ($n$ = 2,3; R = H, Me) as reaction byproducts, while one equivalent of $H_2$ is released per amine-borane equivalent. The processes were followed through multinuclear ($^{31}$P, $^{1}$H, $^{11}$B) variable temperature NMR spectroscopy; kinetic measurements on the hydrogen production rate and the relative rate constants were also carried out. One non-hydridic intermediate could be detected at low temperature, whose chemical nature was explored through a DFT modeling of the reaction mechanism, at the M06//6-31+G(d,p) computational level. The computational output was of help to propose a reliable mechanistic picture of the process.

## Introduction

The increasing quest for efficient and safe hydrogen reservoirs for practical applications in fuel-cells technology within the frame of the so-called "hydrogen economy"[1] has led to an enormous growth of the related hydrogen storage research field in recent years.[2] As far as chemical storage is concerned, one of the most promising materials that can satisfy all the aforementioned requirements is ammonia-borane (AB).[3] In fact, AB is an easy-to-handle solid, it is thermally stable and with a relatively high hydrogen content (19.3% wt H). Homogeneously-catalyzed AB dehydrogenation/hydrolysis is the path that the inorganic chemist can follow to exploit AB as hydrogen storage material. A number of literature examples are known, where $H_2$ evolution is mainly catalyzed by ruthenium,[4] rhodium,[5] and iridium[6] organometallics. Pincer-type metal complexes in particular have been proved to be extremely efficient as alkane dehydrogenation catalysts.[7] Given the isolobal analogy between AB and ethane, some Ir-based pincer systems have been also exploited for AB dehydrogenation.[6f] Group 10 transition metal complexes have been scarcely exploited to achieve this target; to the best of our knowledge, the only literature studies to date are represented by the $Ni^0$-Enders'NHC (1,3,4-triphenyl-4,5-dihydro-1*H*-1,2,4-triazol-5-ylidene) complex[8] that can release more than 2.5 equivalents of $H_2$ per equivalent of AB within 4 h at 60 °C and by the $Pd^{II}$ complex $[Pd(MeCN)_4][BF_4]_2$,[9] releasing up to 2 equivalents of $H_2$ per equivalent of AB within 60 s at room temperature. Some nanostructured $Pd^0$ heterogeneous systems have been also examined for AB dehydrogenation,[10] with comparable results.

Here, amine-borane dehydrogenation/oligomerization by an air-stable robust PCP-pincer $Pd^{II}$ complex [($^{tBu}$PCP)Pd($H_2O$)]$PF_6$ [**2**, $^{tBu}$PCP = 2,6-$C_6H_3(CH_2P^tBu_2)_2$] is described. The expected compound has been generated from the corresponding chloro complex ($^{tBu}$PCP)Pd(Cl) (**1**) after halide abstraction

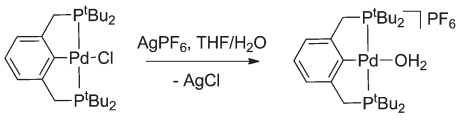


**1** **2**

**Scheme 1** Synthesis of complex **2**.

[a]*Consiglio Nazionale delle Ricerche, Istituto di Chimica dei Composti Organometallici (ICCOM-CNR), Via Madonna del Piano 10, 50019 Sesto Fiorentino (Firenze), Italy. E-mail: a.rossin@iccom.cnr.it*

[b]*Instituto de Investigaciones Químicas, CSIC and Universidad de Sevilla, Av. Américo Vespucio 49, 41092 Sevilla, Spain*

†In memory of Dr Stefano Midollini, in recognition of his remarkable scientific contributions to the growth of the Italian organometallic chemistry.

‡Electronic supplementary information (ESI) available: Fig. S1–S5, complete crystallographic data and tables for **2**, Cartesian *xyz* coordinates and related absolute $G^{THF}$ energy values of **2$^H$_AB**, **2$^H$_AB2**, **2$^H$_BNBN**, **2$^H$_cyc** and [($^H$PCP)-Pd($\eta^2$-$H_2$)]$^+$. CCDC 891104. For ESI and crystallographic data in CIF or other electronic format see DOI: 10.1039/c2dt32273k

with $AgPF_6$ in wet THF (Scheme 1). The $[(^{tBu}PCP)Pd]^+$ fragment, with a coordination vacancy on the metal centre, is rather reactive, and the empty site is easily occupied by water molecules, thus forming the related aquo complex.

## Experimental section

All reactions were performed using the standard Schlenk procedures under a dry nitrogen atmosphere, unless specified. All solvents employed were purged with nitrogen for 10 min before use. The $^{tBu}$PCP(H) ligand (STREM Chemicals Ltd), silver hexafluorophosphate (STREM Chemicals Ltd), ammonium tetrachloropalladate(II) (Aldrich), ammonia-borane complex (Aldrich), dimethylamine-borane complex (Aldrich) and triethylamine-borane complex (Aldrich) were used as purchased, without further treatment. Deuterated solvents (Aldrich) were degassed by three freeze–pump–thaw cycles before use. NMR spectra were recorded on a BRUKER AVANCE II 300 MHz spectrometer, equipped with a low-temperature measurement tool. $^1$H and $^{13}C\{^1H\}$ chemical shifts are reported in parts per million (ppm) downfield of tetramethylsilane (TMS) and were calibrated against the residual protiated resonance of the deuterated solvent ($^1$H) or the deuterated solvent resonance ($^{13}C\{^1H\}$), respectively, while $^{31}P\{^1H\}$ was referenced to 85% $H_3PO_4$ with downfield shift taken as positive. $^{11}$B chemical shifts were referenced to $BF_3{\cdot}OEt_2$. Infrared spectra were recorded with a Perkin-Elmer Spectrum BX FT-IR spectrophotometer. The C, H elemental analyses were made at ICCOM-CNR using a Thermo FlashEA 1112 Series CHNS-O elemental analyzer with an accepted tolerance of ±0.4 units on carbon (C) and hydrogen (H).

### Synthesis of ($^{tBu}$PCP)Pd(Cl) (1)

This compound has already been reported in the literature;[11] in here, an improvement of the original preparation is reported. Ammonium tetrachloropalladate(II) $(NH_4)_2PdCl_4$ (0.14 g, 0.5 mmol) was dissolved in 20 mL 2-methoxyethanol at room temperature. The free ligand $^{tBu}$PCP(H) (0.2 g, 0.5 mmol, 1 equiv.) was added to this solution, and the resulting mixture was heated at 100 °C for 40 min. After that time, the colourless solution was brought to room temperature, and a white crystalline precipitate of pure **1** (0.2 g; yield: 80%) was obtained after concentration to *ca.* 5 mL and addition of 15 mL $H_2O$. The precipitate was filtered, washed with small portions (3 × 10 mL) of an EtOH–$H_2O$ mixture (4 : 1) and finally dried under a brisk nitrogen stream. $^{31}P\{^1H\}$-NMR (121.49 MHz, ppm, $CDCl_3$): 72.1 (s).

### Synthesis of [($^{tBu}$PCP)Pd($H_2O$)]$PF_6$ (2)

0.1 g (0.19 mmol) of **1** were dissolved in 15 mL THF and 0.1 mL $H_2O$. To this solution, 0.06 g (0.22 mmol, 1.2 equiv.) of solid $AgPF_6$ were added in one portion. Immediate formation of a white AgCl precipitate was observed. The suspension was left to stir vigorously overnight at ambient temperature, in the dark. After that time, the colourless supernatant was filtered and concentrated to *ca.* 5 mL under a brisk nitrogen flux. *n*-Pentane addition (10 mL) led to precipitation of **2** as a white crystalline solid, that was washed with small pentane portions (3 × 10 mL) and dried under a nitrogen stream (0.12 g; quantitative yield). Single crystals suitable for X-ray analysis were grown from THF–*n*-pentane solutions at ambient temperature. Anal. Calcd for **2**, $C_{24}H_{45}F_6OP_3Pd$ (662.91): C, 43.48; H, 6.84. Found: C, 43.25; H, 7.01. IR (298 K, KBr, $cm^{-1}$): 3312 w [$\nu$(O–H)], 2960 m, 2900 m, 2870 m [$\nu$(C–H)], 1627 w [$\nu$(C=C)], 1472 m, 1370 m, 1265 m, 1178 m, 1021 m, 963 w, 843 vs [$\gamma$(C–H)], 557 s [$\nu$(P–F)]. $^1$H-NMR (300.13 MHz, ppm, THF-$d_8$, 298 K): 6.95 (Ar*H*, 3H, m), 5.12 ($H_2$O, 2H, s), 3.33 (PC$H_2$, 4H, vt, $^*J_{H-P}$ = 4.1 Hz), 1.40 (C$H_3$, 36H, vt, $^*J_{H-P}$ = 6.9 Hz). $^{13}C\{^1H\}$ NMR (75.46 MHz, ppm, THF-$d_8$, 298 K): 149.7 ($C_{ar\text{-}ipso}$, vt, $^*J_{C-P}$ = 9.8 Hz), 146.4 ($C_{ar\text{-}p}$, s), 124.0 ($C_{ar\text{-}m}$, s), 121.0 ($C_{ar\text{-}o}$, vt, $^*J_{C-P}$ = 10.4 Hz), 32.9 (P*C*H$_2$, vt, $^*J_{C-P}$ = 7.6 Hz), 29.4 [P*C*($CH_3$)$_3$, vt, $^*J_{C-P}$ = 11.2 Hz], 26.6 (PC($CH_3$)$_3$, s). $^{31}P\{^1H\}$-NMR (121.49 MHz, ppm, THF-$d_8$, 298 K): 76.7 (PCP, s), −148.0 ($PF_6$, sept., $J_{P-F}$ = 710.5 Hz).

### X-ray data collection

X-ray data for **2** were collected at low temperature (120 K) on an Oxford Diffraction XCALIBUR 3 diffractometer equipped with a CCD area detector using Mo $K_\alpha$ radiation ($\lambda$ = 0.7107 Å). The program used for the data collections was CrysAlis CCD 1.171.[12] Data reductions were carried out with the program CrysAlis RED 1.171[13] and the absorption corrections were applied with the program ABSPACK 1.17.13. Direct methods implemented in Sir97[14] were used to solve the structures and the refinements were performed by full-matrix least-squares against $F^2$ implemented in SHELX97.[15] All the non-hydrogen atoms were refined anisotropically while the hydrogen atoms were fixed in calculated position and refined isotropically with the thermal factor depending on that of the atom to which they are bound. A different treatment was used for the hydrogen atoms of the *aquo* ligand: they were found in the Fourier density map, the coordinates were free to refine and their thermal factors were bound to that of oxygen. Geometrical calculations were performed by PARST97[16] and molecular plots were produced by the program ORTEP3.[17]

### VT-NMR monitoring of the reaction of 2 with excess $BH_3{\cdot}L$ (L = $NH_3$, $NHMe_2$, $NEt_3$)

Only the reaction of **2** with $BH_3{\cdot}NH_3$ is described, as the other borane adducts were reacted with **2** in an analogous manner. In a typical experiment, **2** (0.040 g, 0.06 mmol) was placed in a 5 mm quartz NMR tube under an inert atmosphere. THF-$d_8$ (0.5 mL) was transferred into the tube *via* a cannula, and the resulting solution was brought to 190 K using a dry ice–acetone bath. 5 equiv. $BH_3{\cdot}NH_3$ (0.0093 g, 0.3 mmol) were dissolved in the minimum amount (0.5 mL) of THF-$d_8$ into a separate Schlenk flask under nitrogen, and the resulting solution was syringed into the cold NMR tube. The tube was then inserted into the NMR spectrometer probe head pre-cooled at 190 K. Subsequently, the probe was warmed slowly to room temperature in steps of 20 K each, and new sets of

 

multinuclear NMR data were collected at each step. In the case of (neat) liquid amine-borane reagents, the required number of equivalents were directly syringed into the pre-cooled NMR tube, always kept at 190 K.

### Kinetic measurements

**(a) $H_2$ evolution rate.** The kinetic runs were carried out with the *Man of the Moon X102* kit (see Fig. S1‡ for details). Under an inert atmosphere, 0.010 g of AB (0.32 mmol) were placed in a two-necked round-bottomed 30 mL flask connected to a switchable three-way valve through a *Torion* screw. AB was dissolved in 1 mL dioxane, stirred at 303 K in an oil bath, then the valve was switched to the pressure transducer which is connected *via* wireless to the software recording the kinetic profile on-line. A stock solution of **2** in the same solvent was added to reach the desired **2** : AB relative stoichiometry (see below) and the reaction was stirred for 18–24 hours. The resulting kinetic data were corrected by the injected volume of catalyst solution: the pressure increase caused by the injection was measured on a blank solution and used to calculate the correct number of released $H_2$ equivalents. At the end of the reaction, the supernatant was transferred to an NMR tube and analyzed through $^{31}P\{^1H\}$ and $^{11}B$ NMR spectroscopy, to identify the soluble reaction by-products.

**(b) Monitoring conversion of AB or DMAB for determination of the reaction rate utilizing $^{11}B$ NMR spectroscopy.** The variation of AB/DMAB concentration during the reaction with **2** at 303 K in THF-$d_8$ was monitored through the integration of the related $^{11}B$ NMR signals. A coaxial external standard of $BF_3{\cdot}Et_2O$ was employed, to have a reference signal for the peaks integration. The NMR tubes were prepared in the same manner as that described above for the VT experiments. In order to avoid sample decomposition, addition of the excess amine-borane (5 equivalents) was made at 190 K and the mixture warmed slowly to 303 K within the probe head of the NMR spectrometer.

### Computational details

Density Functional Theory (DFT) calculations were performed for the AB case only for the sake of simplicity, using the *Gaussian09* program (revision *A.02*).[18] Model structures were optimized with an M06 functional[19] (already employed successfully in other cases for the treatment of molecules containing dative bonds[20]) using the LANL2DZ pseudopotential[21] and related basis set[22] on the palladium and phosphorus atoms, a 6-31G* basis set on all the other pincer atoms and a 6-31+G(d,p) basis set on $BH_3{\cdot}NH_3$. Introduction of diffuse functions is essential to well-reproduce conformational equilibria and experimental electron affinities.[23] An extra p-type polarization function for P and an extra f-type function for Pd were added to the standard set.[22] Gibbs energy calculations to infer relative thermodynamic stabilities were carried out on a *model* system, with the *tert*-butyl groups on the pincer ligand replaced by H atoms ($^H$PCP), in order to reach a satisfactory compromise between model system accuracy and short computational times. Evaluation of the solvent effects was performed through a continuum modelling of the reaction medium. Bulk solvent effects (THF, $\varepsilon$ = 7.42) were expressed through the SMD Continuum Model,[24] with the same basis set used for the gas phase optimizations. Gibbs energy in solution was calculated according to the following simplified equation:

$$G_{THF} = G_{gas} + (E_{THF} - E_{gas})$$

## Results and discussion

### Synthesis and characterization of the catalytic species

The synthesis of the chloro complex ($^{tBu}$PCP)Pd(Cl) **1** was carried out through the direct reaction of ammonium tetrachloropalladate(II) $(NH_4)_2PdCl_4$ and the commercially available $^{tBu}$PCP(H) in 2-methoxyethanol, with concomitant *in situ* C–H bond activation and $HCl/NH_4Cl$ elimination. The reaction yield has been slightly improved (from 75 to 80%) with respect to the original literature report,[11] where the benzonitrile adduct *cis*-$PdCl_2(PhCN)_2$ as a $Pd^{II}$ source was employed instead. Halide abstraction from **1** with $AgPF_6$ in wet THF led to the isolation of the air-stable compound [($^{tBu}$PCP)Pd($H_2O$)]-$PF_6$ (**2**); the *aquo* ligand though is rather labile and it can be easily replaced by other small molecules that enter the metal coordination sphere. Nevertheless, no replacement of the coordinated water molecule with other neutral coordinating species (acetonitrile, carbon monoxide[25]) was attempted, since these species may be reactive towards amine-boranes, while water is *kinetically and thermodynamically inert* under the reaction conditions employed in our study (*vide infra*); this has also been confirmed by the computational results.[26] **2** has been thoroughly characterized through multinuclear ($^{31}P$, $^1H$, $^{13}C$) NMR and IR spectroscopy; single crystals suitable for X-ray diffraction were grown from THF–*n*-pentane solutions. The compound crystallizes in the monoclinic $P2_1$ space group (Fig. 1); the coordination geometry at the $Pd^{II}$ centre is (distorted) square planar {[$\alpha$(P(1)–Pd–P(2)] = 166.02(3)°; $\alpha$[P(1)–Pd–O(1)] = 96.86(9)°; $\alpha$[P(1)–Pd–C(1)] = 83.48(9)°}; the structural parameters {$d$[Pd–C(1)] = 2.026(3) Å; $d$[Pd–P(1)] = 2.314(1) Å;

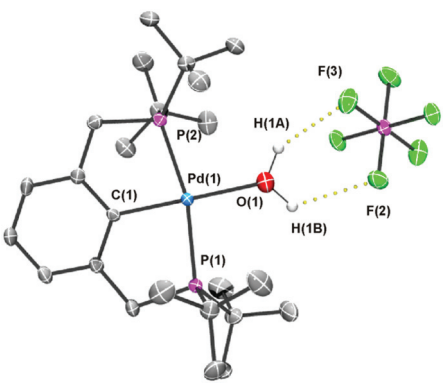


**Fig. 1** ORTEP diagram (thermal ellipsoids at 50% probability) of the asymmetric unit in the crystal lattice of **2**. Hydrogen atoms on the ligand omitted for clarity. Hydrogen bonds depicted as yellow dotted lines. See the ESI‡ for the complete set of crystallographic parameters and tables.

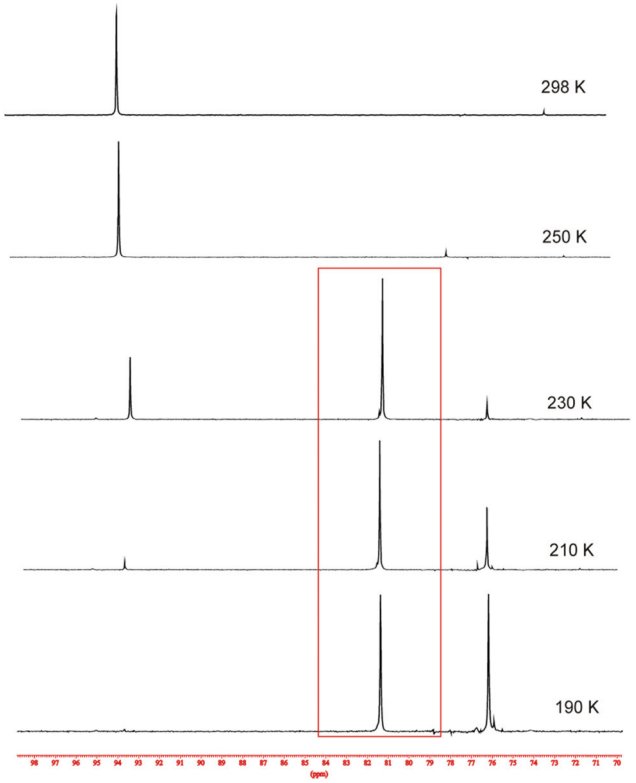


**Fig. 2** $^{31}P\{^{1}H\}$ VT-NMR spectra of the **2** : AB mixture (1 : 5 stoichiometry, THF-$d_8$). The red box highlights the signal of the reaction intermediate detected between 190 and 230 K.

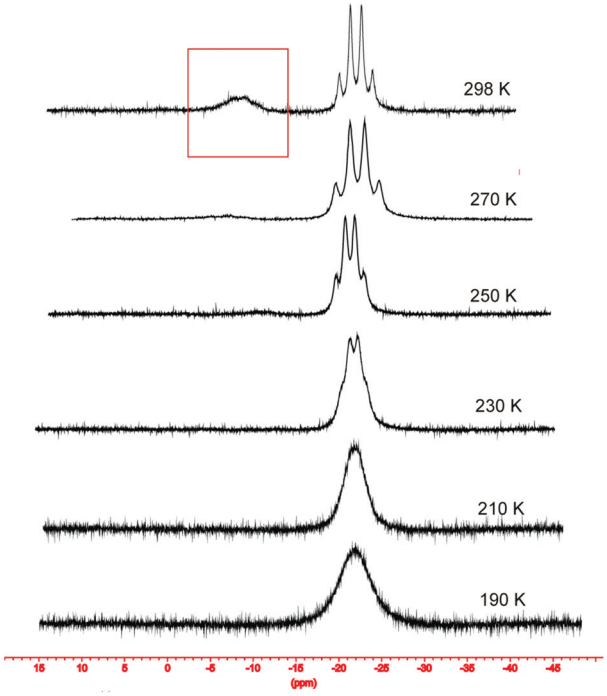


**Fig. 3** $^{11}B$ VT-NMR spectra of the **2** : AB mixture (1 : 5 stoichiometry, THF-$d_8$). The red box highlights the signal of the oligomeric product obtained during the dehydrogenation process.

*d*[Pd–O(1)] = 2.157(3) Å} are very similar to those of other species containing the $[(^{tBu}PCP)Pd]^+$ fragment.[27] The $PF_6^-$ counterion is hydrogen-bonded to the coordinated *aquo* ligand {*d*[F(2)···H(1B)] = 2.51(5) Å; *d*[F(3)···H(1A)] = 2.24(5) Å; *α*[F(2)···H(1B)–O(1)] = 109(3)°; *α*[F(3)···H(1A)–O(1)] = 142(4)°}.

### Variable temperature multinuclear NMR analysis

The reaction of **2** with 5 equivalents of AB in THF-$d_8$ was followed *via* multinuclear $^{31}P$, $^{1}H$ and $^{11}B$ variable-temperature (VT) NMR spectroscopy in the 190–298 K temperature range. At 190 K the only species present in the $^{31}P\{^{1}H\}$ NMR spectra besides the starting material is a non-hydridic intermediate at $\delta_P$ = 81 ppm (Fig. 2); above 230 K, a slow conversion of this species into the hydride compound ($^{tBu}$PCP)Pd(H) ($\delta_P$ = 94.4 ppm; $\delta_H$ = −4.2 ppm, $^{1}J_{H-P}$ = 13.7 Hz)[11,28] occurred. During the same reaction time, an off-white polymeric precipitate was also formed at the bottom of the NMR tube. The soluble dehydrogenation by-products are tentatively assigned to oligomeric species of general formula $[BH_2–NH_2]_n$ ($n$ = 2–3),[29] as suggested by the $^{11}B$-NMR peak centered at $\delta_B$ = −12.1 ppm recorded in the supernatant solution (Fig. 3). It appears as a very broad pseudo-quartet, resulting from the overlapping of two triplets falling at close chemical shifts (this has been confirmed by the $^{11}B\{^{1}H\}$ spectra, where two broad singlets are observed at $\delta_B$ = −11.6 and $\delta_B$ = −12.7 ppm. The presence of two peaks is likely to be related to the different chain size, since early literature reports[29b] stated that the cyclic and linear isomers are indistinguishable in the $^{11}B$-NMR spectra). Unfortunately, all the attempts made to isolate the pure products failed. The solid precipitate has been investigated by IR spectroscopy: it probably consists of a mixture of unidentified longer-chain $[BH_2–NH_2]_n$ oligomers of the same type as those present in solution [the adsorption bands related to the $\nu(BH_2)$, $\nu(NH_2)$ and $\nu$(B–N) normal modes were observed at 3284, 2425 and 1458 $cm^{-1}$, respectively;[30] the exact chemical composition though could not be determined]. After 18 h at ambient temperature, not all the excess of AB was converted into oligomers; a complete conversion could not be achieved, while the starting catalyst turned into the thermodynamically stable hydride species ($^{tBu}$PCP)Pd(H) quantitatively. This is also in agreement with the kinetic results (*vide infra*). It is likely that the monohydride species represents the "spent catalyst", as confirmed by its direct reactivity with AB (1 : 5), which did not lead to any $H_2$ production and/or AB oligomerization.

The reaction with the *N*-substituted amine-borane DMAB (in the same 1 : 5 stoichiometric ratio) proceeded through a reaction mechanism that seems to be the same as that of AB; again, at low temperatures a peak falling at $\delta_P$ = 82.0 ppm was detected in the $^{31}P\{^{1}H\}$ NMR spectrum, that slowly disappears turning into the ($^{tBu}$PCP)Pd(H) complex (Fig. S2‡); at the end of the catalysis, the cyclic dimer *cyclo*-$[BH_2–NMe_2]_2$ was the main species observed in the $^{11}B$ NMR spectrum as a triplet at $\delta_B$ = 5.9 ppm ($^{1}J_{B-H}$ = 113.4 Hz, Fig. S3‡).[31] No unreacted DMAB was detected at room temperature after 18 h; at odds with what was found for AB, complete conversion of DMAB to

 

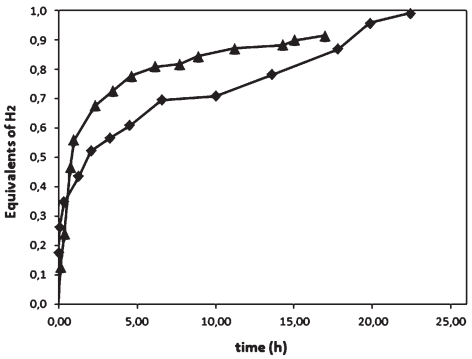


**Fig. 4** $H_2$ evolution in the AB dehydrogenation process catalyzed by **2** (303 K, dioxane) for different **2** : AB ratios (◆, 1 : 5; ▲, 1 : 20).

oligomers was achieved. No evidence of formation of the ethylene analogue $BH_2{=}NMe_2$ was found, either coordinated to the metal centre or free in solution (at odds with other literature cases[4d,f,5a,b,i,l]), presumably because of the fast dimerization process.

No reaction occurred between **2** and triethylamine borane $NEt_3{\cdot}BH_3$ (always in a 1 : 5 ratio); only the unreacted starting materials were observed in the NMR spectra, at all temperatures. This confirms that hydrogen is directly produced from the amine-borane dehydrogenation.

### Quantitative $H_2$ determination

The kinetic profiles at 303 K of the AB dehydrogenation reaction were also determined, for different (**2** : AB) stoichiometric ratios (Fig. 4). In the (1 : 5) case, the reaction was completed after *ca.* 22 h, and one $H_2$ equivalent per AB equivalent was released. Analysis through $^{11}B$ NMR of the supernatant solution at the end of the reaction did not show unreacted AB, in contrast with the observation made in the VT NMR experiment; this is probably due to the different hydrogen concentration in the two experiments. Indeed, under these experimental conditions, *ca.* 50% of **2** is still present at the end of the process. In agreement with that, the increase of AB concentration in the reaction causes a release of less $H_2$ equivalents and a more rapid catalyst deactivation [*i.e.* formation of ($^{tBu}$PCP)Pd(H)]. Thus, with a (1 : 20) ratio, around 0.9 $H_2$ equivalents per AB equivalent are released before all the metal complex has been transformed into ($^{tBu}$PCP)Pd(H), with some AB being unreacted in the final solution. In contrast, running the reaction with a (1 : 50) ratio, the amount of $H_2$ equivalents released is never higher than 0.4–0.5, with unreacted monomer in the final solution, this indicating a quicker catalyst deactivation.

The measurement of the amount of $H_2$ released in the reaction with DMAB following this approach was proved to be not feasible. The volatility of the corresponding spent fuel *cyclo*-$[BH_2{-}NMe_2]_2$ [32] provided an exceedingly high value of the total gas pressure recorded; it was not possible to quantify the contribution given by each of the two species. Nonetheless, it is reasonable to assume that a maximum of one $H_2$ equivalent

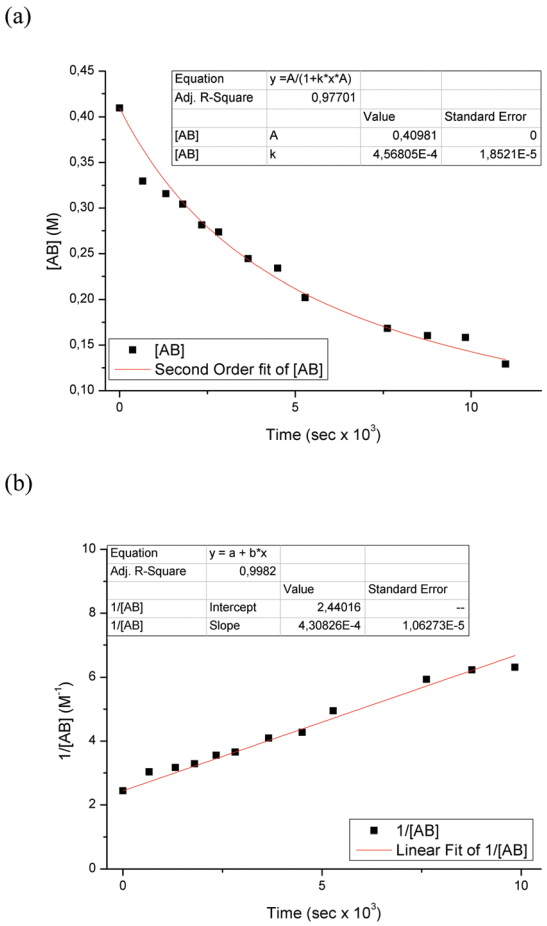


**Fig. 5** (a) Linear [AB] *vs.* *t* and (b) normalized 1/[AB] *vs.* *t* plots (second order rate law) for the AB dehydrogenation reaction catalyzed by **2** (303 K, THF-$d_8$).

per monomer equivalent is released also in this case, according to the $^{11}B$ NMR analysis of the spent fuel (see previous paragraph and Fig. S3‡).

### Kinetic measurements and evaluation of the reaction rate through $^{11}B$ NMR spectroscopy

For the sake of comparison, the kinetic rate constant ($k_{obs}$) values for the dehydrogenation of AB and DMAB by **2** at 303 K were determined through $^{11}B$ NMR monitoring. The competitive reaction of nascent $H_2$ with the palladium fragment to produce the "spent form" ($^{tBu}$PCP)Pd(H) is responsible for the variation of the active catalyst concentration in time; consequently, for a more reliable evaluation of the rate constants, only the data points collected within the initial 3 h were taken into account for the fitting, assuming that the catalyst concentration is constant within this time range. The results were plotted as a 1/[AB] *vs.* *t* graph (Fig. 5), assuming a *second order* kinetic rate law with respect to AB: $-d[AB]/dt = k_{obs}[AB]^2$. The assumption comes from the results of the DFT mechanistic analysis (*vide infra*), where the only reaction step showing a positive $\Delta G$ value is that related to the adduct between the $[(^{H}PCP)Pd]^+$ fragment and *two* molecules of AB. In order to verify this hypothesis, an initial rate experiment was

performed on the reaction between **2** and AB (see ESI‡ for details). The results confirmed the second order in substrate concentration. Following the second order data fitting, a final $k_{obs}$ value of 4.31(11) × $10^{-4}$ $M^{-1}$ $s^{-1}$ is obtained for AB. As for DMAB, the same approximation led to a $k_{obs}$ value of 2.67(5) × $10^{-4}$ $M^{-1}$ $s^{-1}$ (Fig. S4‡). The reaction rate is higher for AB than for DMAB, probably because of a predominant steric hindrance of the secondary amine with respect to ammonia that reasonably makes dimerization slower.

### DFT modeling of the AB dimerization mechanism

The results coming from the VT-NMR studies prompted us to cast light on the reaction mechanism through DFT modeling, at the M06//6-31+G(d,p) computational level. For the sake of simplicity, only the formation of *cyclo*-$(BH_2–NH_2)_n$ ($n$ = 2) was taken into account in the computational modeling of the reaction mechanism. To this aim, a simplified structure for **2** was taken into account for the thermodynamics calculations, where the bulky *tert*-butyl groups were replaced with hydrogen atoms, to achieve the best compromise between model system accuracy and computational time.[33] The resulting [($^{H}$PCP)Pd-($H_2O$)]$^+$ cation $\mathbf{2^H}$ was assumed to be the starting complex. The overall proposed catalytic cycle for the AB dimerization reaction with formation of the inorganic cyclobutane analogue $[BH_2–NH_2]_2$ and two equivalents of $H_2$ ($\Delta G$ = −12.0 kcal $mol^{-1}$, Scheme 2) is reported in Scheme 3. Due to the complex nature of the mechanistic steps involved in this process, no transition states could be found along the reaction coordinate; therefore, only the $\Delta G$ values (thermodynamics) for each step have been assessed in THF.

The *aquo* complex $\mathbf{2^H}$ readily undergoes ligand exchange with one molecule of AB, to form an $\eta^1$-BH-bonded adduct $\mathbf{2^H}$**_AB** (Fig. 6).[26] The interaction of AB with the [($^{H}$PCP)Pd]$^+$ fragment is weak, but the exchange process is thermodynamically downhill, with a $\Delta G$ of −7.5 kcal $mol^{-1}$. No stabilizing interaction of the ammonia-borane N–H bonds with the [($^{H}$PCP)Pd]$^+$ fragment was found, in line with what was already observed in other cases of cationic transition metal moieties.[9,6c] It is proposed that the labile intermediate observed in the $^{31}P\{^1H\}$ NMR spectra in the variable-temperature experiments could be represented by the simple adduct between [($^{tBu}$PCP)Pd]$^+$ and AB, with the same structure as $\mathbf{2^H}$**_AB**.

Interaction of $\mathbf{2^H}$**_AB** with an additional AB molecule leads to the adduct $\mathbf{2^H}$**_AB2** (Fig. 7), with a *positive* Gibbs energy variation of +4.9 kcal $mol^{-1}$. The entropy reduction while passing from ($\mathbf{2^H}$**_AB** + AB) to $\mathbf{2^H}$**_AB2** is a plausible reason for this step to be endoergonic. The presence of the second AB molecule favors the coordination slippage of the Pd-bound AB from

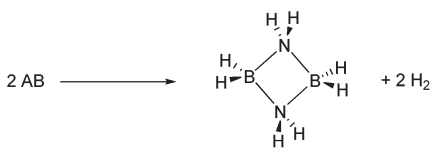


**Scheme 2** Cyclo-dimerization of AB.

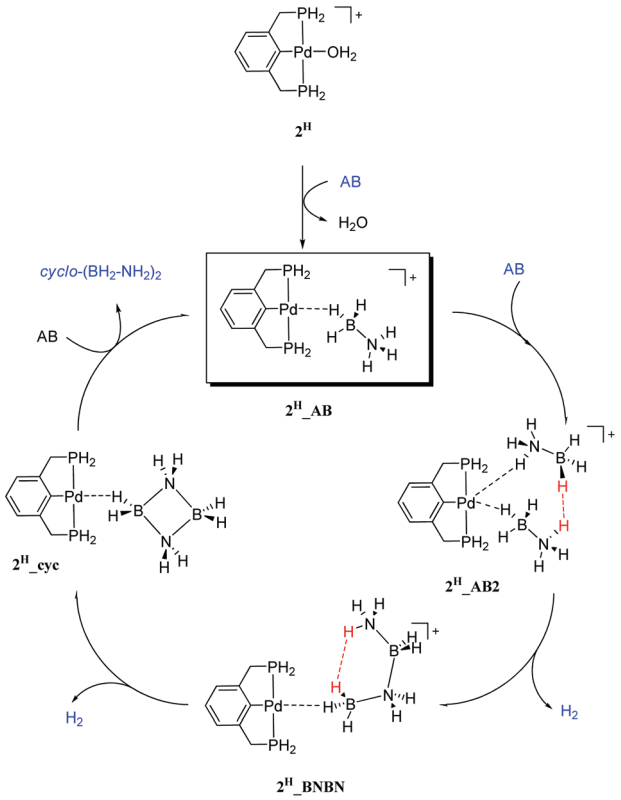


**Scheme 3** Proposed catalytic cycle for AB cyclo-dimerization in the presence of **2**. The dihydrogen bonding between hydridic and protonic H atoms is shown in red. Reactants and products are drawn in blue.

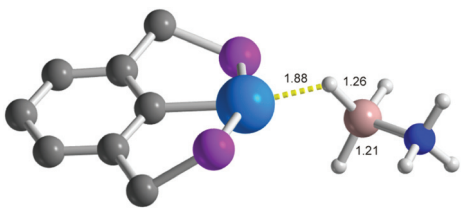


**Fig. 6** Optimized geometry of [($^{H}$PCP)Pd($\eta^1$-AB)]$^+$ ($\mathbf{2^H}$**_AB**). Selected optimized bond lengths reported (Å). H atoms on the pincer ligand omitted for clarity. Atom color code: white, H; gray, C; purple, P; blue, N; pink, B; light blue, Pd.

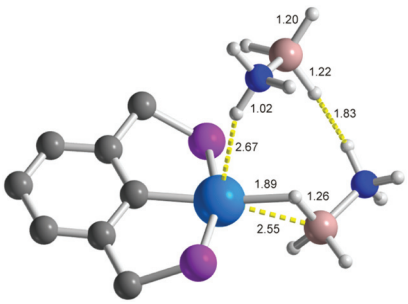


**Fig. 7** Optimized geometry of [($^{H}$PCP)Pd(σ-*BH*-AB)···AB]$^+$ ($\mathbf{2^H}$**_AB2**). Selected optimized bond lengths reported (Å). H atoms on the pincer ligand omitted for clarity. Atom color code: see Fig. 6. N–H···H–B dihydrogen bonds and σ-BH agostic interactions drawn as yellow dotted lines.

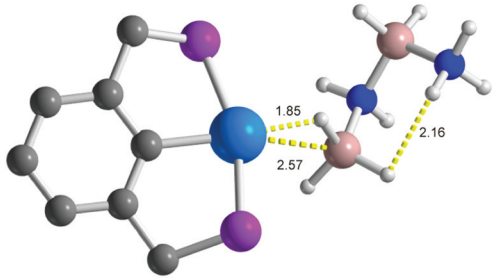


**Fig. 8** Optimized geometry of $[(^{H}PCP)Pd(\sigma\text{-}BH\text{–}BH_3\text{–}NH_2\text{–}BH_2\text{–}NH_3)]^+$ (**$2^{H}$_BNBN**). Selected optimized bond lengths reported (Å). H atoms on the pincer ligand omitted for clarity. Atom color code: see Fig. 6. N–H···H–B dihydrogen bonds and σ-BH agostic interactions drawn as yellow dotted lines.

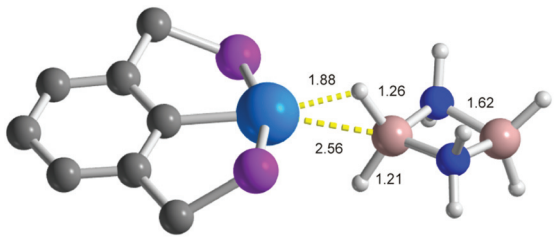


**Fig. 9** Optimized geometry of $\{(^{H}PCP)Pd[\sigma\text{-}BH\text{-}cyclo\text{-}(BH_2NH_2)_2]\}^+$ (**$2^{H}$_cyc**). Selected optimized bond lengths reported (Å). H atoms on the pincer ligand omitted for clarity. Atom color code: see Fig. 6. σ-BH agostic interactions drawn as yellow dotted lines.

$\eta^1$-BH to σ-BH agostic. This reveals that both coordination modes at the $Pd^{II}$ cation are possible, and the σ-agostic geometry can be considered a sort of "transition state" between different $\eta^1$-BH modes of the *fluxional* AB "ligand".[34] Dihydrogen B–H···H–N bonding between the two monomers is present [optimized *d*(B–H···H–N) = 1.83 Å]. A weak N–H interaction of the non-coordinated monomer with the metal centre is also present [optimized *d*(N–H···Pd) = 2.67 Å].

At this stage, a metal-mediated AB dimerization may occur, with formation of one equivalent of $H_2$ and the linear $BH_3$–$NH_2$–$BH_2$–$NH_3$ dimer (the inorganic butane analogue, which was also independently prepared and characterized)[35] coordinated to palladium, *i.e.* the $[(^{H}PCP)Pd(\eta^1\text{-}BH\text{–}BH_3\text{–}NH_2\text{–}BH_2\text{–}NH_3)]^+$ adduct (**$2^{H}$_BNBN**, Fig. 8). The $\Delta G$ for this step equals −13.5 kcal $mol^{-1}$.

Further intramolecular dehydrogenation (promoted by the existence of an intramolecular dihydrogen bonding in **$2^{H}$_BNBN**, as evidenced in Fig. 8) leads to $[(^{H}PCP)Pd(\eta^1\text{-}BH\text{-}cyclo\text{-}(BH_2\text{–}NH_2)_2]^+$ (**$2^{H}$_cyc**, Fig. 9), where the stabilizing σ-BH agostic interaction provides $\Delta G$ = −1.1 kcal $mol^{-1}$. At this stage, replacement of the cyclic dimer by another AB "monomer" ($\Delta G$ = −2.2 kcal $mol^{-1}$) regenerates the starting active species **$2^{H}$_AB** for another catalytic run. During the reaction course catalyst deactivation progressively occurs, through direct interaction of **$2^{H}$** with nascent $H_2$ and subsequent formation of the non-classical hydride $[(^{H}PCP)Pd(\eta^2\text{-}H_2)]^+$ (Fig. S5‡). This reaction is almost thermoneutral ($\Delta G$ = + 0.8 kcal $mol^{-1}$). Despite the lack of experimental evidence for the existence of such an unstable and reactive dihydrogen compound {only the platinum(II) analogue $[(^{tBu}PCP)Pt(\eta^2\text{-}H_2)]^+$ was experimentally synthesized through protonation of the classical $(^{tBu}PCP)Pt(H)$ and detected in the $^1H$ NMR spectrum at very low temperatures (180 K)[36]} and the scarcity of genuine non-classical Pd molecular hydrogen complexes, it can be possibly invoked as the transient precursor of the final classical monohydride.

## Conclusions

In summary, amine-borane dehydrogenation/oligomerization mediated by the robust palladium (PCP)-pincer complex $[(^{tBu}PCP)Pd(H_2O)]PF_6$ has been studied through a combination of experimental (VT-NMR, kinetic profiles) and computational (DFT) techniques, with the aim of unraveling reaction intermediates and the amount of $H_2$ produced under the applied experimental conditions. At odds with other $Pd^{II}$-based systems,[9] the pincer compound examined produces only one $H_2$ equivalent per AB equivalent. This reveals a limited dehydrogenation ability that leads to "aliphatic" rather than "aromatic" (borazine-like) oligomers as a spent fuel. At the same time, this finding can be seen as an advantage from an engineering point of view, since in hydrogen fuel cells technology significant efforts are being made to reduce or eliminate borazine as a detrimental side-product. Besides, these mechanistic studies are of fundamental importance in light of the development of better-performing homogeneous catalysts for an efficient AB dehydrogenation. Novel pincer-type transition metal organometallics are currently being prepared in our laboratories, with the aim of testing them as novel amine-borane dehydrogenation catalysts.

## Acknowledgements

The PIRODE project of the Italian Ministry of the Environment, the EFOR project of the Italian National Research Council, the Spanish Ministry of Science (projects CTQ2010-17476 and Consolider-Ingenio 2010 CSD2007-00006) and the Junta de Andalucía (project P09-FQM-4832) (FEDER support) are acknowledged for financial support. The CNR–CSIC bilateral agreement is acknowledged for mobility funding through the "Chemical hydrogen storage: amino boranes activation with transition metal organometallics" project (CSIC 2010IT0036, CNR 11544). A. M. L.-V. thanks the CSIC and ESF for support through the JAE-doc program. The use of the computational facilities of the Centre de Serveis Científics i Acadèmics de Catalunya (CESCA) is greatly appreciated. Thanks are also given to the project Firenze Hydrolab-2 supported by ECRF.

## Notes and references

1 (*a*) R. Lan, J. T. S. Irvine and S. Tao, *Int. J. Hydrogen Energy*, 2012, **37**, 1482–1494; (*b*) T. Umegaki, J.-M. Yan,

X.-B. Zhang, H. Shioyama, N. Kuriyama and Q. Xu, *Int. J. Hydrogen Energy*, 2009, **34**, 2303–2311; (*c*) D. Wenger, W. Polifke, E. Schmidt-Ihn, T. Abdel-Baset and S. Maus, *Int. J. Hydrogen Energy*, 2009, **34**, 6265–6270.

2 U. Eberle, M. Federhoff and F. Schueth, *Angew. Chem., Int. Ed.*, 2009, **48**, 6608–6630 and references therein.

3 (*a*) S. Udishnu, U. B. Demirci, B. R. Jagirdar and P. Miele, *ChemSusChem*, 2011, **4**, 1731–1739; (*b*) T. Hügle, M. Hartl and D. Lentz, *Chem.–Eur. J.*, 2011, **17**, 10184–10207; (*c*) A. Staubitz, A. P. M. Robertson and I. Manners, *Chem. Rev.*, 2010, **110**, 4079–4124; (*d*) N. C. Smythe and J. C. Gordon, *Eur. J. Inorg. Chem.*, 2010, 509–521; (*e*) F. H. Stephens, V. P. Pons and R. T. Baker, *Dalton Trans.*, 2007, 2613–2626; (*f*) T. B. Marder, *Angew. Chem., Int. Ed.*, 2007, **46**, 8116–8118.

4 (*a*) C. J. Wallis, H. Dyer, L. Vendier, G. Alcaraz and S. Sabo-Etienne, *Angew. Chem., Int. Ed.*, 2012, **51**, 3646–3648; (*b*) B. L. Conley, D. Guess and T. J. Williams, *J. Am. Chem. Soc.*, 2011, **133**, 14212–14215; (*c*) G. Alcaraz and S. Sabo-Etienne, *Angew. Chem., Int. Ed.*, 2010, **49**, 7170–7179; (*d*) G. Alcaraz, L. Vendier, E. Clot and S. Sabo-Etienne, *Angew. Chem., Int. Ed.*, 2010, **49**, 918–920; (*e*) M. Käβ, A. Friedrich, M. Drees and S. Schneider, *Angew. Chem., Int. Ed.*, 2009, **48**, 905–907; (*f*) A. Friederich, M. Drees and S. Schneider, *Chem.–Eur. J.*, 2009, **15**, 10339–10342; (*g*) N. Blacquiere, S. Diallo-Garcia, S. I. Gorelsky, D. A. Black and K. Fagnou, *J. Am. Chem. Soc.*, 2008, **130**, 14034–14035.

5 (*a*) L. J. Sewell, G. C. Lloyd-Jones and A. S. Weller, *J. Am. Chem. Soc.*, 2012, **134**, 3598–3610; (*b*) C. Y. Tang, N. Phillips, J. I. Bates, A. L. Thompson, M. J. Gutmann and S. Aldridge, *Chem. Commun.*, 2012, **48**, 8096–8098; (*c*) C. Y. Tang, A. L. Thompson and S. Aldridge, *Angew. Chem., Int. Ed.*, 2010, **49**, 921–925; (*d*) G. Alcaraz, A. B. Chaplin, C. J. Stevens, E. Clot, L. Vendier, A. S. Weller and S. Sabo-Etienne, *Organometallics*, 2010, **29**, 5591–5595; (*e*) A. B. Chaplin and A. S. Weller, *Inorg. Chem.*, 2010, **49**, 1111–1121; (*f*) A. B. Chaplin and A. S. Weller, *Angew. Chem., Int. Ed.*, 2010, **49**, 581–584; (*g*) R. Dallanegra, A. B. Chaplin and A. S. Weller, *Angew. Chem., Int. Ed.*, 2009, **48**, 6875–6878; (*h*) T. M. Douglas, A. B. Chaplin, A. S. Weller, X. Yang and M. B. Hall, *J. Am. Chem. Soc.*, 2009, **131**, 15440–15456; (*i*) M. E. Sloan, T. J. Clark and I. Manners, *Inorg. Chem.*, 2009, **48**, 2429–2435; (*j*) T. M. Douglas, A. B. Chaplin and A. S. Weller, *J. Am. Chem. Soc.*, 2008, **130**, 14432–14433; (*k*) T. J. Clark, G. R. Whittell and I. Manners, *Inorg. Chem.*, 2007, **46**, 7522–7527; (*l*) Y. Chen, J. L. Fulton, J. C. Linehan and T. Autrey, *J. Am. Chem. Soc.*, 2005, **127**, 3254–3255.

6 (*a*) H. C. Johnson, A. P. M. Robertson, A. B. Chaplin, L. J. Sewell, A. L. Thompson, M. F. Haddow, I. A. Manners and A. S. Weller, *J. Am. Chem. Soc.*, 2011, **133**, 11076–11079; (*b*) R. Ciganda, M. A. Garralda, L. Ibarlucea, E. Pinilla and M. Rosario Torres, *Dalton Trans.*, 2010, **39**, 7226–7229; (*c*) T. W. Graham, C.-W. Tsang, X. Chen, R. Guo, W. Jia, S.-M. Lu, C. Sui-Seng, C. B. Ewart, A. Lough, D. Amoroso and K. Abdur-Rashid, *Angew. Chem., Int. Ed.*, 2010, **49**, 8708–8711; (*d*) A. Rossin, M. Caporali, L. Gonsalvi, A. Guerri, A. Lledós, M. Peruzzini and F. Zanobini, *Eur. J. Inorg. Chem.*, 2009, 3055–3059; (*e*) A. Paul and C. B. Musgrave, *Angew. Chem., Int. Ed.*, 2007, **46**, 8153–8156; (*f*) M. C. Denney, V. Pons, T. J. Hebden, M. Heinekey and K. I. Goldberg, *J. Am. Chem. Soc.*, 2006, **128**, 12048–12049.

7 (*a*) *The Chemistry of Pincer Compounds*, ed. D. Morales-Morales and C. M. Jensen, Elsevier, Amsterdam NL, 2007; (*b*) I. Göttker-Schnetmann, P. White and M. Brookhart, *J. Am. Chem. Soc.*, 2004, **126**, 1804–1811; (*c*) K. Krogh-Jespersen, M. Czerw, N. Summa, K. B. Renkema, P. D. Achord and A. S. Goldman, *J. Am. Chem. Soc.*, 2002, **124**, 11404–11416.

8 (*a*) X. Yang and M. B. Hall, *J. Am. Chem. Soc.*, 2008, **130**, 1798–1799; (*b*) R. J. Keaton, J. M. Blacquiere and R. T. Baker, *J. Am. Chem. Soc.*, 2007, **129**, 1844–1845.

9 S.-K. Kim, W.-S. Han, T.-J. Kim, T.-Y. Kim, S. W. Nam, M. Mitoraj, Ł. Piekoś, A. Michalak, S.-J. Hwang and S. O. Kang, *J. Am. Chem. Soc.*, 2010, **132**, 9954–9955.

10 (*a*) Ö. Metin, S. Duman, M. Dinç and S. Özkar, *J. Phys. Chem. C*, 2011, **115**, 10736–10743; (*b*) R. P. Shrestha, H. V. K. Diyabalanage, T. A. Semelsberger, K. C. Ott and A. K. Burrell, *Int. J. Hydrogen Energy*, 2009, **34**, 2616–2621.

11 C. J. Moulton and B. L. Shaw, *J. Chem. Soc., Dalton Trans.*, 1976, 1020–1024.

12 *CrysAlisCCD 1.171.31.2 (release 07-07-2006), CrysAlis171. NET*, Oxford Diffraction Ltd.

13 *CrysAlis RED 1.171.31.2 (release 07-07-2006), CrysAlis171. NET*, Oxford Diffraction Ltd.

14 A. Altomare, M. C. Burla, M. Camalli, G. L. Cascarano, C. Giacovazzo, A. Guagliardi, A. G. G. Moliterni, G. Polidori and R. Spagna, *J. Appl. Crystallogr.*, 1999, **32**, 115.

15 G. M. Sheldrick, *SHELXL*, 1997.

16 M. Nardelli, *Comput. Chem.*, 1993, **7**, 95.

17 L. J. Farrugia, *J. Appl. Chem.*, 1999, **32**, 837.

18 M. J. Frisch, *et al.*, *GAUSSIAN 09 (Revision A.02)*, Gaussian Inc., Wallingford CT, 2009.

19 Y. Zhao and D. G. Truhlar, *Theor. Chem. Acc.*, 2008, **120**, 215–241.

20 Y. Zhao and D. G. Truhlar, *Acc. Chem. Res.*, 2008, **41**, 157–167.

21 (*a*) P. J. Hay and W. R. Wadt, *J. Chem. Phys.*, 1985, **82**, 270–283; (*b*) W. R. Wadt and P. J. Hay, *J. Chem. Phys.*, 1985, **82**, 284–298.

22 (*a*) A. Höllwarth, M. Böhme, S. Dapprich, A. W. Ehlers, A. Gobbi, V. Jonas, K. F. Köhler, R. Stegmann, A. Veldkamp and G. Frenking, *Chem. Phys. Lett.*, 1993, **208**, 237–240; (*b*) A. W. Ehlers, M. Böhme, S. Dapprich, A. Gobbi, A. Höllwarth, V. Jonas, K. F. Köhler, R. Stegmann, A. Veldkamp and G. Frenking, *Chem. Phys. Lett.*, 1993, **208**, 111–114.

23 B. J. Lynch, Y. Zhao and D. G. Truhlar, *J. Phys. Chem. A*, 2003, **107**, 1384–1388.

24 A. V. Marenich, C. J. Cramer and D. G. Truhlar, *J. Phys. Chem. B*, 2009, **113**, 6378–6396.

 

25 Literature examples containing the $[(^{tBu}PCP)M(L)]^+$ cationic fragment are: (*a*) $[(^{tBu}PCP)Ni(MeCN)]^+$: V. A. Levina, A. Rossin, N. V. Belkova, M. R. Chierotti, L. M. Epstein, O. A. Filippov, R. Gobetto, L. Gonsalvi, A. Lledòs, E. S. Shubina, F. Zanobini and M. Peruzzini, *Angew. Chem., Int. Ed.*, 2011, **50**, 1367–1370; (*b*) $[(^{tBu}PCP)Pt(CO)]^+$: D. Vuzman, E. Poverenov, Y. Diskin-Posner, G. Leitus, L. W. Y. Shimon and D. Milstein, *Dalton Trans.*, 2007, 5692–5700.

26 The direct reaction of AB with the coordinated water molecule did not lead to reasonable $\Delta G$ values in some steps of the (supposed) catalytic cycle, providing a very unfavorable overall thermodynamics. Indeed, no experimental evidence of reaction between AB or DMAB and $H_2O$ was found, under the applied experimental conditions [*i.e.* absence of $^{11}B$ NMR signals typical of boric acid-like hydrolysis products (to be expected around $\delta_B$ = +18.0 ppm)]. From all these findings, this hypothesis was discarded.

27 $[(^{tBu}PCP)Pd(H_2O)]BF_4$: B. F. M. Kimmich, W. J. Marshall, P. J. Fagan, E. Hauptman and R. M. Bullock, *Inorg. Chim. Acta*, 2002, **330**, 52–58. $(^{tBu}PCP)Pd(NO_2)$/$(^{tBu}PCP)Pd(NO_3)$: R. Johansson, L. Ohrstrom and O. F. Wendt, *Cryst. Growth Des.*, 2007, **7**, 1974–1979. $(^{tBu}PCP)Pd(CH_3)$: R. Johansson, M. Jarenmark and O. F. Wendt, *Organometallics*, 2005, **24**, 4500–4502. $(^{tBu}PCP)Pd(OCOCF_3)$: M. T. Johnson, M. Cetina, K. Rissansen and O. F. Wendt, *Acta Crystallogr., Sect. E: Struct. Rep. Online*, 2010, **66**, m675.

28 M. C. Denney, N. A. Smythe, K. L. Cetto, R. A. Kemp and K. I. Goldberg, *J. Am. Chem. Soc.*, 2006, **128**, 2508–2509.

29 (*a*) W. J. Shaw, J. C. Linehan, N. K. Szymczak, D. J. Heldebrant, C. Yonker, D. M. Camaioni, R. T. Baker and T. Autrey, *Angew. Chem., Int. Ed.*, 2008, **47**, 7493–7496; (*b*) J. S. Wang and R. A. Geanangel, *Inorg. Chim. Acta*, 1988, **148**, 185–190.

30 K. W. Böddeker, S. G. Shore and R. K. Bunting, *J. Am. Chem. Soc.*, 1966, **88**, 4396–4401.

31 (*a*) H. J. Cowley, M. S. Holt, R. L. Melen, J. M. Rawson and D. S. Wright, *Chem. Commun.*, 2011, **47**, 2682–2684; (*b*) T. Beweries, J. Thomas, M. Klahn, A. Schulz, D. Heller and U. Rosenthal, *ChemCatChem*, 2011, **3**, 1865–1868.

32 C. A. Jaska, K. Temple, A. J. Lough and I. Manners, *Chem. Commun.*, 2011, 962–963.

33 An assessment of the computational error made when passing from the real to the model system was made on the gas phase $\Delta E$ values for the exchange reaction $[(^{R}PCP)Pd(H_2O)]^+ + AB \rightarrow [(^{R}PCP)Pd(AB)]^+ + H_2O$. The results were the following: R = $^{t}$Bu, $\Delta E$ = −8.3 kcal mol$^{-1}$; R = H, $\Delta E$ = −11.5 kcal mol$^{-1}$. Thus, the same order of magnitude of the thermodynamic reaction parameters is calculated when replacing the (real) *tert*-butyl substituents on phosphorus with hydrogen atoms.

34 This kind of fluxional coordination hapticity (that translates into *magnetically equivalent* H atoms in the $^1H$ NMR spectra) has also been observed for transition metal *borohydride* complexes, such as: (*a*) $(PPh_3)_2Cu(BH_4)$: I. E. Golub, O. A. Filippov, E. I. Gutsul, N. V. Belkova, L. M. Epstein, A. Rossin, M. Peruzzini and E. S. Shubina, *Inorg. Chem.*, 2012, **51**, 6486–6497; (*b*) $(^{tBu}PCP)Ni(BH_4)$: A. Rossin, M. Peruzzini and F. Zanobini, *Dalton Trans.*, 2011, **40**, 4447–4452.

35 X. Chen, J.-C. Zhao and S. G. Shore, *J. Am. Chem. Soc.*, 2010, **132**, 10658–10659.

36 B. F. M. Kimmich and R. M. Bullock, *Organometallics*, 2002, **21**, 1504–1507.